Soil Dynamics and Earthquake Engineering 104 (2018) 174–185

Contents lists available at ScienceDirect

Soil Dynamics and Earthquake Engineering

journal homepage: www.elsevier.com/locate/soildyn

Modeling added spatial variability due to soil improvement: Coupling FEM with binary random fields for seismic risk analysis

Silvana Montoya-Noguera[a,b,*], Fernando Lopez-Caballero[a]

[a] MSSMat, CNRS, CentraleSupélec, Paris-Saclay University, 92290 Châtenay-Malabry, France
[b] Current institution: Department of Civil Engineering, Universidad EAFIT, Medellín, Colombia

ARTICLE INFO

Keywords:
Seismic liquefaction
Soil improvement
Spatial variability
Homogenization

ABSTRACT

A binary mixture homogenization model is proposed for predicting the effects on liquefaction-induced settlement after soil improvement based on the consideration of the added spatial variability between the natural and the treated soil. A 2D finite element model of an inelastic structure founded on a shallow foundation was coupled with a binary random field. Nonlinear soil behavior is used and the model is tested for different mesh size, model parameters and input motions.

Historical evidence as well as physical and numerical modeling indicate that improved sites present less liquefaction and ground deformation. In most cases this improvement is modeled as homogeneous; however, in-situ measurements evidence the high level of heterogeneity in the deposit. Inherent spatial variability in the soil and the application of some soil improvement techniques such as biogrouting and Bentonite permeations will necessary introduce heterogeneity in the soil deposit shown as clusters of the treated material in the natural soil. Hence, in this study, improvement zones are regarded as a two-phase mixture that will present a nonlinear relation due to the level of complexity of seismic liquefaction and the consequent settlement in a structure. This relation is greatly affected by the mechanical behavior of the soils used and the input motion. The effect on the latter can be efficiently related to the equivalent wave period as the proposed homogenization model depends on the stiffness demand of the input motion.

1. Introduction

Soil improvement techniques such as biogrouting and Bentonite permeations are becoming widely used to strengthen soils and mitigate liquefaction. Significant advances have been made in the equipment and methods used although, the high degree of spatial variability introduced in the design and its effect of the system's performance are less known [1]. The success of these techniques is related to two factors: (1) the effectiveness of the method related to how much of the soil is being changed – and (2) the efficiency in improving the soil behavior related to how much are the consequences optimized. The effectiveness can be measured by the spatial fraction of the treated soil with respect to the total treatment area, for example the amount of gravel, clay or bacteria introduced in a sand deposit. However, the efficiency is related to the different spatial configurations on the vertical as well as in the horizontal direction which will present an important uncertainty in the response. A success function relating effectiveness and the average efficiency could be defined in order to optimize the soil improvement consequences.

For obtaining an average behavior of the improved ground, a homogenization method has to be defined. In this paper, to analyze the effects of added spatial variability due to soil improvement techniques, binary random fields are coupled to a 2D finite element model (FEM) with soil-structure interaction. The former is used to generate the treated ground soil as a two-phase mixture composed of the reference soil and the added improved material. The latter is a two-story inelastic structure with a shallow foundation on loose-to-medium sand (LMS). In the treatment zone, a medium-to-dense sand (MDS) is added. Montoya-Noguera and Lopez-Caballero [2] analyzed the effect of the different spatial distributions on the interactions between the two materials as it

Abbreviation: D_{5-95}, Predominant duration; EQ, Earthquake; FEM, Finite element model; FF, Free-field; f_{str}, Fundamental frequency; GEM, Generalized Effective Medium; IM, Intensity measures; I_A, Arias intensity; LMS, Loose-to-medium sand; MDS, Medium-to-dense sand; PHA, Peak horizontal acceleration; PHV, Peak horizontal velocity; p_w, Fluid pore pressure; $|u_z|$, Relative surface settlement of the structure with respect to FF; SSI, Soil-structure interaction; TF, Transfer function; $T_{V/A}$, Period of equivalent harmonic wave; V_s, Shear wave velocity; $V_{s\,30}$, Geometric mean of V_s for the upper 30 m; β_1, β_2, Horizontal and vertical auto-regressive coefficients; Δp_w, Excess pore pressure; $\Delta|u_z|$, Relative difference of $|u_z|$; γ, Spatial fraction; γ_c, Critical spatial fraction; κ, Hydraulic conductivity (or permeability); ξ, Damping

* Corresponding author at: Department of Civil Engineering, Universidad EAFIT, Medellín, Colombia
E-mail addresses: smontoyan@eafit.edu.co (S. Montoya-Noguera), fernando.lopez-caballero@centralesupelec.fr (F. Lopez-Caballero).

http://dx.doi.org/10.1016/j.soildyn.2017.10.009
Received 11 March 2016; Received in revised form 24 July 2017; Accepted 16 October 2017
Available online 05 November 2017

changes the pore-pressure migration and average liquefaction in the model. The present study extends the work in three main directions:

1. The relation between the technique effectiveness and the average efficiency, defined as the success function, is evaluated for different input motions. To measure the efficiency, the relative surface settlement of the structure with respect to free-field ($|u_z|$) at the end of shaking is used.
2. Investigating the sensitivity of the analysis regarding the mesh size discretization and the material's behavior.
3. The success function is related to different homogenization theories. First traditional theories regarding only the geometry of the mixture are tested and finally an advanced method is proposed.

1.1. Soil improvement and soil mixtures

There are not many real-size experimental observations for reduction of liquefaction potential with spatial measures showing the distribution of treated zones. Even if in reality, grouted columns are designed to have specific diameters and spacings, the material is in most cases an heterogeneous mixture of the added soil (or material) and the original one. Generally, it is difficult to measure the mechanical properties of these columns in the field. Lambert et al. [3] performed laboratory tests in samples from soil-cement mixed columns and found heterogeneities in the sides as well as in the core of the columns, that consequently affected the mechanical properties. Different studies have assessed the fraction of soil remaining in the columns, for example Boulanger et al. [4] estimated it at about 20%.

DeJong et al. [5,6] presented results of large-scale and centrifuge tests of bio-grouting. Resistivity in-situ measurements were evaluated before and after bio-grouting. Before improvement, soil variability appears to be continuous and the horizontal correlation is considerately higher than the vertical correlation. After treatment, some areas present more bacteria-induced cementation and a clear distinction is shown between clusters or pockets. Centrifuge tests presented by DeJong et al. [5] also show the clusters of modified soil in a discrete distribution. This distribution might be caused by clogging of the soil pore spaces and more calcite near the injection point [7].

Evidence of the decrease of liquefaction resistance of the mixture compared to that of uniform samples is found in undrained cyclic triaxial tests on sand-gravel [8] and sand-silt [9] mixtures and centrifuge tests on mixtures of sand with different densities [10,11] and with different permeabilities [12]. In general, it was found that the effect of the loose sand zone was to induce increased excess pore water pressure (Δp_w) in the surrounding dense sand or create drainage paths, through which the Δp_w can be drained out causing differential settlements. Most of these studies have dealt with the liquefaction triggering and have not evaluated the response of structures underlying liquefiable soil deposits or the liquefaction-induced settlements.

1.2. Homogenization theories

The process of homogenization consists of deriving the effective properties for an heterogeneous system so that it can be viewed as homogeneous on a particular macroscopic scale depending on the property of interest [13]. The effective medium depends on the *geometry* (e.g. shape and size of particles) and the *topology* or connectivity among particles. A brief description of the homogenization theories used in this study is presented below:

1.2.1. Traditional theories

Traditional homogenization theories are often used to describe geotechnical properties. For example, the work on spatial variability effect on bearing capacity of Popescu et al. [14] often compares the average results of the heterogeneous soil models with the "corresponding homogeneous soil". According to the authors, the homogenization is the mean value of the Monte Carlo simulations; although this is only true for vertically layered materials (i.e. parallel to the bearing capacity) described by classical homogenization theories. If, on the contrary, the layers are horizontal (i.e perpendicular or serial) the effective properties of the homogeneous model would be a harmonic average. It is clear that for random fields, these are only extreme cases which are known as Wiener [15] bounds. For a mixture of properties D_1 and D_2 where is the spatial fraction of D_2, the Wiener [15] bounds are defined as:

- Parallel:

$$D_{\parallel} = (1-\gamma)\cdot D_1 + \gamma \cdot D_2$$

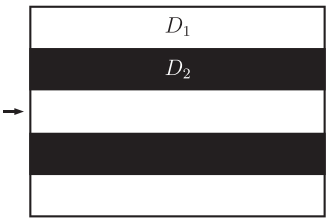

- Serial:

$$D_{\perp} = \frac{1}{\frac{(1-\gamma)}{D_1} + \frac{\gamma}{D_2}}$$

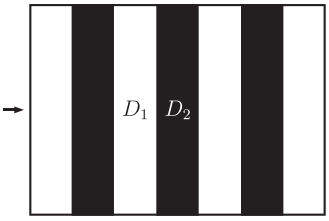

Another case that can be exactly modeled as homogeneous consists of concentric-shell structures, i.e. one material coating the other in spheres of different size. When $D_2 > D_1$, the properties can be described by the HS equation expressed by Hashin and Shtrikman [16] as:

- Material 1 coating material 2:

$$D_{HS^+} = D_2 + \frac{1-\gamma}{\frac{1}{D_1 - D_2} + \frac{\gamma}{d \cdot D_2}}$$

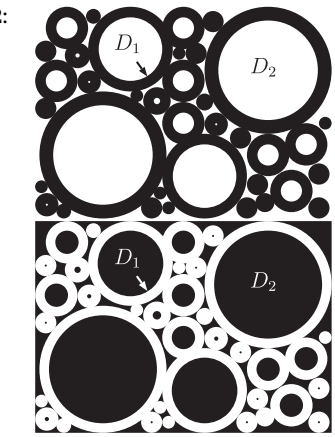

- Material 2 coating material 1:

$$D_{HS^-} = D_1 + \frac{\gamma}{\frac{1}{D_2 - D_1} + \frac{1-\gamma}{d \cdot D_1}} \quad (4)$$

where d is the dimensionality. This parameter binds the model to fluctuate between the Wiener bounds; hence, when d is equal to unity, they become the parallel bound and as it tends to infinity it approaches the perpendicular one. Actually, HS bounds are narrower than the Wiener bounds and are often used as they are simple and intuitive. However, they still give wide predictions, specially if the ratio between the material properties is big.

1.2.2. Generalized effective medium (GEM)

Traditional homogenization theories are based on the geometric arrangements among the phases, e.g. parallel and series [15] or

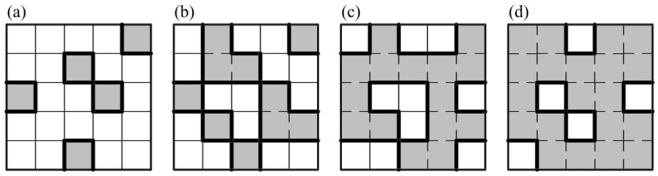

Fig. 1. Example of the percolation types on a discrete random field: (a) $\gamma < \gamma_c^{bond}$, (b) $\gamma = \gamma_c^{bond}$, (c) $\gamma = \gamma_c^{site}$ and (d) $\gamma > \gamma_c^{site}$ (after [18]).

concentric [16]. Effective medium theories (EMT) are derived on the exact solution for a single spherical inclusion in an infinite medium therefore also neglect interactions among particles. However, percolation theories as statistical tools have been developed to describe the topology of heterogeneous materials. They are derived from probabilistic studies of connected clusters of one material in a heterogeneous system [17].

The percolation theory is focused on the existence of a percolating cluster that connects opposite sides of a system. Two types of percolation processes can be identified in lattices as shown in Fig. 1 given by Bunde and Kan–telhardt [18]: the bond, related to the junctions or paths (marked with bold lines), and the site percolation, related to the nearest-neighbors or elements (marked with dashed lines). The first emergence of the percolation cluster corresponds to the critical fraction (γ_c, often noted by p_c but to keep consistency in the case study will be used instead). The specific value of the threshold for elastic materials depends on: the lattice type which includes dimensionality and symmetry, the percolation type, the system size (being finite or infinite), and the correlations among the materials [19].

Exact solutions exist for some systems that correspond to elastic properties of infinitely large non correlated occupations. For example, for a square lattice the exact bond percolation is 0.5 and for site percolation it is slightly higher (about 0.59). When the system is not sufficiently large, there is a range of fractions, spanning over a certain width, in which the percolation transition can possibly occur. As the system size increases, Δ decreases and γ_c approaches the infinite value. When positive correlations exist, more clusters will be formed and γ_c tends to decrease. When in a square lattice, the next-nearest-neighbor is considered in site percolation, γ_c decreases to about 0.41 [20].

When a perfect phase contrast is present, that is the property of interest of one of the two materials is either zero or infinite, the percolation theory describes the effective properties as:

$$D_{eff} \propto (\gamma - \gamma_c)^t \quad \text{for} \quad \gamma > \gamma_c \quad , \quad 0 \quad \text{otherwise}$$
$$D_{eff} \propto (\gamma_c - \gamma)^{-s} \quad \text{for} \quad \gamma < \gamma_c \quad , \quad \infty \quad \text{otherwise}$$

As in most cases, no perfect phase contrast is present, an approximation defined for all values is required. McLachlan et al. [21] derived a semi-empirical correlation that includes the effective diffusivity in EMT. They replaced the dimensionality by the inverse of the percolation threshold (i.e. $1/\gamma_c$) and introduced the exponents s and t. The resulting equation is known as the generalized effective medium (GEM) equation:

$$(1-\gamma)\frac{D_1^{1/s} - D_{eff}^{1/s}}{D_1^{1/s} + (\gamma_c^{-1} - 1)D_{eff}^{1/s}} + \gamma\frac{D_2^{1/t} - D_{eff}^{1/t}}{D_2^{1/t} + (\gamma_c^{-1} - 1)D_{eff}^{1/t}} = 0 \tag{4}$$

where s and t are the scaling exponents for $\gamma < \gamma_c$ and $\gamma > \gamma_c$, respectively. They are universal percolation quantities and are supposedly independent on the discrete or percolation type, the size nor the correlation of the system. Their values can be found via numerical simulations and if certain physical processes can be described by the same set of scaling exponents, then the physical laws governing these phenomena must be fundamentally the same [22]. Although Eq. (4) is semi-empirical, it has been shown both experimentally and numerically to yield good predictions for many transport properties when dealing with binary heterogeneous materials [23].

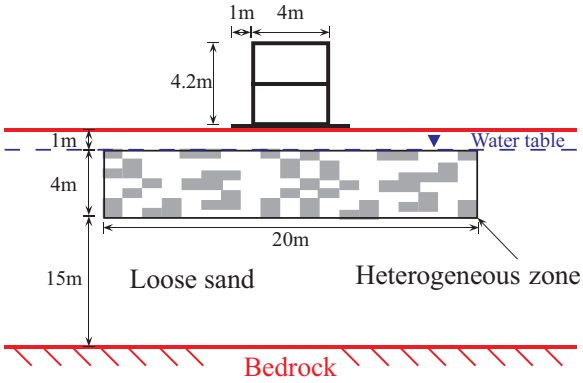

Fig. 2. Schema of the numerical model.

2. Numerical model

The numerical model used in this work corresponds to the reinforced concrete building with a shallow rigid foundation standing on saturated cohesionless soil presented in Montoya-Noguera and Lopez-Caballero [2]. A schema of the model is shown in Fig. 2. The reference soil deposit is a 50 m wide model composed of 20 m of loose-to-medium sand (LMS) overlaying an elastic bedrock. The shear modulus increases with depth. The fundamental elastic period of the soil profile is equal to 0.38 s. An elastoplastic multi-mechanism model is used to represent the soil behavior. Under the deposit, an engineering bedrock representing a half-space medium is modeled with an isotropic linear elastic behavior and a shear wave velocity (V_s) equal to 1700 m/s. The ground water table is located 1 m below the surface.

Concerning the treated ground soil the recommendations of Mitchell et al. [24] were used. The soil heterogeneity is simulated with a binary auto-regressive model composed of two materials: a treated medium-to-dense sand (MDS) and the original loose-to-medium sand (LMS). A brief description of this model is given in Section 2.5. For more information on the model refer to Montoya-Noguera and Lopez-Caballero [2].

2.1. Finite element model

A 2D dynamic approach derived from the $\underline{u}$–p_w version of the Biot's generalized consolidation theory [25] was adopted for the soil. The general purpose finite element code GEFDyn [26] was used. The model uses quadrilateral isoparametric elements with eight nodes for both solid displacements and fluid pressures. The size of the elements in the vertical direction is 0.5 m and in the horizontal direction is 1 m under the heterogeneous zone and 1.5 m on the sides. This element size is in agreement with the minimum number of points per wavelength recommended in the literature to prevent numerical dispersion even for strong motion excitations [27,28]. For the minimum initial V_s in the deposit of 135 m/s near the surface and a maximum frequency of 20 Hz of engineering interest in this study, a minimum of 27 points per wavelength is allowed in the elastic domain. The number of points is high, although it will decrease as the soil softens and the V_s decreases. An implicit Newmark numerical integration scheme is used in the dynamic analysis for the discretization in time. For this case, the induced numerical damping is 0.1%, according to Montoya-Noguera and Lopez-Caballero [29] and corresponding to the scheme parameters: $\gamma_N = 0.611$ and $\beta_N = 0.301$. It is worth mentioning that this numerical damping affects principally the elastic response of the model (i.e. for shear strains less than $1{\cdot}10^{-5}$), while for higher strains the damping is provided by the material degradation as will be shown in Section 2.4. To take into account the interaction effects between the structure and the soil, a modified width plane-strain condition was assumed in the finite element model [30]. In this case a width of 4 m is used for the soil deposit.

As the medium is considered as an infinite semi-space and the wave propagation is only one-dimensional and purely vertical, only incident shear waves propagating in the vertical direction are used as loading. For the bedrock's boundary condition, paraxial elements simulating "deformable unbounded elastic bedrock" have been used [31]. Hence, the incident waves, defined at the outcropping bedrock, are introduced into the base of the model after deconvolution; in other words, the obtained movement at the bedrock interface is composed of both the incident and the reflected waves. Because of the nonlinear model used for the soil behavior, traditional absorbent elements cannot be used on the lateral boundaries. Instead and because the lateral limits are considered to be far enough, the tied-approach proposed by Zienkiewicz et al. [32] is used to reduce the boundary effects. This approach consists of imposing equivalent – or periodic – conditions between the lateral boundaries by tying the nodes at opposite sides and at the same depth to equal normal stress and equal displacements in all directions. It imposes a shear-beam like deformed shape for vertically incident waves similar to a standard 1D seismic vertical propagation. This procedure has been used in nonlinear soil-structure interaction models by Lopez-Caballero and Modaressi-Farahmand-Razavi [33], Saez et al. [30], Sáez and Ledezma [34], Ayoubi and Pak [35]. Similar dynamic behavior was evidenced near the lateral boundaries with and without the structure and the heterogeneous zone.

2.2. Input earthquake motion

The computational cost of many random field simulations is important, hence a careful selection was performed to have strong input motions appropriate for the numerical model. As a deformable bedrock is used and the hypothesis of outcropping rock recordings is made, the earthquake signals should be near-to-source strong motions from dense soil stations. These signals are supposed to have minimal noise at high frequencies. The selected earthquake motions and some intensity measures (IM) are shown in Table 1. The IM shown are the peak horizontal acceleration (PHA), the Arias intensity (I_A), the predominant duration (D_{5-95}) and the peak horizontal velocity (PHV). Fig. 3 shows the normalized response spectra of the signals with a structural damping (ξ) of 5%. As the motions differ greatly in PHA, the results have been normalized in order to emphasize the differences in the frequency content. EQ2 and EQ4 present energy at periods above 1 s and have the maximum duration. Two other motions with similar PHA values but different energy content were tested: EQ3 and EQ6. The latter has the same PHA value and predominant period as EQ4 but lacks the high period energy content. The last motion, EQ 9, is only used in Section 3.2 as an additional test case.

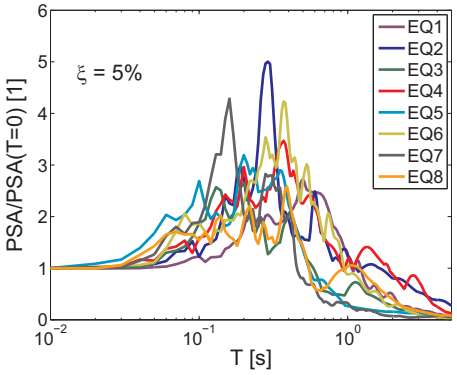

Fig. 3. Normalized response spectra of acceleration.

2.3. Structural model

For the sake of simplicity a two-story reinforced concrete (RC) building proposed by Vechio and Emara [36] is used. It consists of a large-scale one-span model with a shallow rigid foundation, standing on saturated cohesionless soil. The total structure height is 4.2 m and the width is 4.0 m. The mass of the building is equal to 45 T and is assumed to be uniformly distributed along beam elements, while the columns are supposed massless. The foundation is modeled as a rigid block of 0.1 × 6 × 4 m. Between the structure's foundation and the soil, interface elements are used to allow relative movement of the structure with respect to the soil, in order to avoid the traction effect. These elements follow a Coulomb-type plastic criterion.

A scaled motion with a very low amplitude (i.e. PHA ≈ $1{\cdot}10^{-5}$ g) was used to evaluate the pseudo-elastic behavior of both soil and structure. The transfer function is the ratio between two acceleration wave fields and it gives information solely of the system between these two points. Fig. 4 shows the transfer function (TF) of the free-field (surface/bedrock) and of the structure at fixed base and with soil-structure interaction (SSI) effects (top/FF). Regarding the structure, it can be seen that even if the building has two stories it behaves like a single-degree-of-freedom, as the second amplification peak is above 15 Hz and of significantly less amplitude. The fundamental frequency (f_{str}), corresponding to the first peak, is equal to 4.16 Hz. The SSI effect results on a shift of the main structure's frequency and a deamplification due to the flexibility of the foundation soil and the material and radiation damping added by the soil. In quasi-elastic conditions, shown in the figure, the material damping is low and this effect is primarily due to the flexibility of the structure with respect to that of the soil. In this

Table 1
Input motions' identification and some intensity measures.

#	Event	Year	RSN*	M_w	R_{JB} † [km]	$V_{s\,30}$ [m/s]	PHA [g]	I_A [m/s]	D_{5-95} [s]	PHV [cm/s]
EQ1	Northridge_01	1994	1050	6.69	4.9	2016	0.43	1.79	9.84	51.23
EQ2	Kocaeli, Turkey	1999	1165	7.51	3.6	811	0.21	0.80	13.3	34.64
EQ3	Friuli, Italy_02	1976	133	5.91	14.4	660	0.23	0.22	2.83	12.5
EQ4	Irpinia, Italy	1980	292	6.9	6.78	382	0.25	1.19	15.07	36.40
EQ5	Loma Prieta	1989	765	6.93	9.64	1428	0.41	1.05	6.53	31.57
EQ6	Northridge_01	1994	1012	6.69	9.87	706	0.25	0.93	8.07	27.39
EQ7	Loma Prieta	1989	810	6.93	18.41	714	0.40	2.04	9.66	17.53
EQ8	San Fernando	1971	77	6.61	1.81	2016.1	1.18	8.59	6.68	103.23
EQ9	Loma Prieta	1989	763	6.93	9.96	729.7	0.32	0.68	4.64	20.66

*Record sequence number at the NGA database (http://ngawest2.berkeley.edu/)
† Joyner-Boore source-to-site distance.

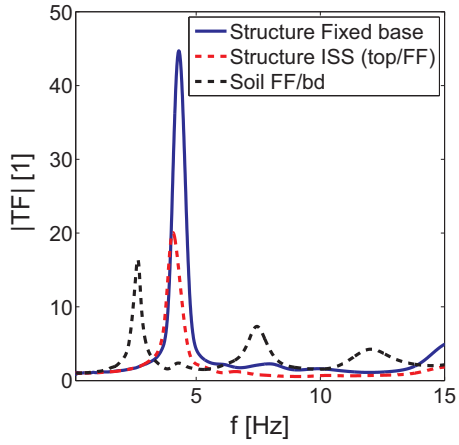

Fig. 4. Transfer function of the structure with fixed base and with SSI effect (top/FF) and of the soil deposit at free-field (surface/bedrock).

case, the SSI effects are significant with almost 50% deamplification as the structure is more flexible than the soil (which presents a fundamental frequency of 3.7 Hz).

2.4. Soil constitutive model

The soil behavior is simulated with the ECP elasto-plastic multi-mechanism model, which is an advanced step-by-step integration model developed at *CentraleSupélec* in the early 80 s [37–39]. The model is written in terms of effective stresses, uses a Coulomb type failure criterion and follows the critical state concept. The evolution of hardening is based on the plastic strain (deviatoric and volumetric strains for the deviatoric mechanisms and only volumetric strains for the isotropic one). To take into account the cyclic behavior it uses a kinematical hardening which relies on the state variables, at the last load reversal. The soil behavior is decomposed into pseudo-elastic, hysteretic and mobilized domains hence it can take into account a large range of deformations. For a complete understanding of the ECP model refer to Hujeux [40] and Modaressi [38], among others.

The ECP model has been validated for different kinds of loading and the main results are shown in many publications; among others, Costa D'Aguiar et al.[41], Saez et al. [30] for reproducing laboratory tests, Foerster and Modaressi [42], Bernardie et al. [43] for seismic soil response of vertical arrays, and Sica et al. [44] for seismic response of soil structures.

For this application the treated zone is composed of two materials: a treated medium-to-dense sand (MDS) and the original loose-to-medium sand (LMS). Their model parameters were calibrated using the procedures defined by Lopez-Caballero et al. [45] and Carrilho Gomes et al. [46]. The validation of the LMS and MDS model parameters with different laboratory tests were performed independently by Lopez-Caballero and Modaressi-Farahmand-Razavi [47] and Saez [48], respectively. The deeper layers are also taken from Lopez-Caballero and Modaressi-Farahmand-Razavi [47]. The model parameters for both soils are shown in Table 2. These parameters are divided into five groups corresponding to the different mechanisms. The parameters that are undirectly measured are geometric parameters that allow the calibration of different laboratory tests. Some laboratory tests simulations can be found in Montoya-Noguera and Lopez-Caballero [2]. It should be noted that the ECP model regards the initial relative densities as consequence of some intrinsic soil parameters, e.g. the soil density and the porosity, the initial state given by the critical stress and the void ratio. The hydraulic conductivity (κ) is initially different for the two soils: $1{\cdot}10^{-4}$ m/s for LMS and $1{\cdot}10^{-5}$ m/s for MDS. These values were taken from the literature of the soil model's calibration and their influence in the response will be evaluated in Section 3.1.

Table 2
ECP model parameters.

Parameter	MDS	LMS	[5-10]m	[10-15]m	[15-20]m
Solid density (ρ_s) [kg/m^3]	2700				
Initial porosity (n_0) [1]	0.35	0.47			
Coefficient of earth pressure (k_0) [1]	0.6				
Hydraulic conductivity (κ) [m/s]	$1{\cdot}10^{-5}$	$1{\cdot}10^{-4}$			
Elasticity					
Bulk modulus (K_{ref}) [MPa]	444	628			
Shear modulus (G_{ref}) [MPa]	222.4	290.0			
Nonlinear exponent (n_e) [1]	0.4	0.5			
Reference mean stress (p_{ref}) [MPa]	1.0				
Critical State and Plasticity					
Friction angle (ϕ'_{pp}) [°]	31	30			
Plastic compressibility modulus (β) [1]	43	33			
Isotropic consolidation distance (d) [1]	3.5	2.0			
Yield surface shape* (b) [1]	0.20				
Initial critical stress (p_{co}) [MPa]	1.800	0.019	0.040	0.061	0.082
Flow Rule and Isotropic Hardening					
Characteristic angle (ψ) [°]	31	30			
Volumetric parameter* (α_ψ) [1]	1.0				
Primary plastic stiffness* (a_1) [1]	0.0001				
Secondary plastic stiffness* (a_2) [1]	0.004	0.002			
Monotonic isotropic hardening* (c_1) [1]	0.03	0.001			
Cyclic isotropic hardening* (c_2) [1]	0.06	0.002			
Cyclic loading exponential* (m) [1]	1.0	1.5			
Threshold Domains					
Elastic* (r^{ela}) [1]	0.005	0.03	0.02	0.01	0.005
Hysteretic* (r^{hys}) [1]	0.03	0.04			
Mobilized* (r^{mob}) [1]	0.8				
Isotropic elastic* (r^{ela}_{iso}) [1]	0.001				

* Undirectly measured. Refer to Lopez-Caballero et al. [45] and Carrilho Gomes et al. [46].

The model considers an isotropic and nonlinear elasticity domain, where the bulk (K) and the shear (G) moduli are functions of the mean effective stress (p') and an exponent coefficient dictating the degree of nonlinearity (n_e). In this case, even if the reference moduli and n_e of LMS are larger than those of MDS, the maximum shear and bulk moduli are larger for the MDS in the zone of treatment. Overall, the maximum shear and bulk moduli profiles vary only slightly between the two soils; however, their behavior changes with increasing nonlinear effects. Hence in order to analyze the differences concerning the liquefaction resistance, an undrained stress controlled cyclic shear test was simulated. The cyclic stress ratio ($SR = \tau/\sigma'_{v0}$) as a function of the number of loading cycles to produce liquefaction (N) is shown in Fig. 5 for both soils at varying effective initial consolidation pressures (p'_0): 50, 80 and 100 kPa. As a qualitative comparison, the modeled test results are compared with the curves given by El Mohtar et al. [49] for a clean sand and a sand with 3% of bentonite permeations. It is noted that the obtained curves are closer to the reference for a clean sand corresponding to the LMS; while, the MDS curves are closer to those of a treated soil.

2.5. Binary random field model

The random field is generated with the homogeneous auto-logistic model derived by Bartlett and Besag [50]. It is a nearest-neighbor model defined as a conditional probability. That means it treats dependence directly through the so-called *autocovariate*, i.e. a function of the observations themselves. The binary mixture used to model the heterogeneous zone is defined with the spatial fraction $\gamma = N_1/(N_1 + N_2)$ where N_m is the number of elements of material m. From an engineering point of view, is related, for example, to the efficiency of a soil improvement technique, such as soil-mixing. Thus, could be calculated from the injected material with respect to the total area of intervention. Following the one-sided approximation, the expectation of x_{ij}, a value

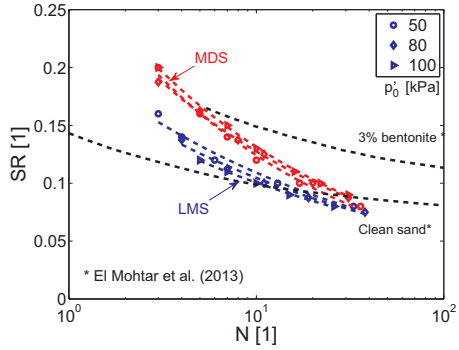

Fig. 5. Simulated liquefaction curves compared with results from El Mohtar et al. [49] for both soils used.

of the binary random variable X_{ij}, is given by:

$$E[x_{ij}|x_{i-1,j}, x_{i,j-1}] = \left[1 - \frac{1}{2}(\beta_1 + \beta_2)\right]\cdot\gamma + \frac{1}{2}(\beta_1\cdot x_{i-1,j} + \beta_2\cdot x_{i,j-1}) \quad (4)$$

where β_1 and β_2 are the auto-regressive coefficients that control the correlation length (λ_c) in the horizontal and vertical direction, and i and j are the horizontal and vertical indices of the elements, respectively. The autocorrelation function ρ_{ij} is equal to $\beta_1^i \cdot \beta_2^j$ as shown in Fig. 6a. Note that when i and j are equal to 1, ρ_{ij} is equal to the product of the correlations (i.e. β^2), thus, it is said that it presents one step correlation in each direction. The correlation structure shows an exponential decay which is expected as it follows the Markov definition of order 1. The exponential function is defined as $\rho_\tau = \exp(-2\tau/\lambda_c)$, where τ is the lag distance. The value of λ_c of the exponential function is related to β as follows: $\lambda_c = -2/\ln(\beta^2)$. Note that the indices and the auto-regressive coefficients are normalized by the number and size of the elements corresponding to the β value used, in Fig. 6b λ_c is dimensionalized for the present case as a function of β in the horizontal and vertical directions. For each element, the generated probability is not a binary number, so it is compared to a random number that follows a uniform distribution function between 0 and 1, where each element is independent. This process, known as binarization, makes use of Monte Carlo simulations to converge to a given value. Further details on this model are presented in Montoya-Noguera and Lopez-Caballero [2].

3. Results

The added spatial variability due to soil improvement is modeled with the binary random field described in Section 2.5. Different effectiveness levels of the improvement technique are tested by varying the spatial fraction () between not treated to fully treated (i.e. from 1 to 0) and 50 independent spatial distributions per value were realized. In this analysis, both auto-regressive coefficients (β_1 and β_2) are equal to 0.4 (i.e. a correlation length close to 8.7 m in the horizontal direction and 1.7 m in the vertical direction, as shown in Fig. 6b). This value was taken from in-situ measurements and recommendations for sandy soil and gravelly sand [51,52]. It is worth noting that the case of injected columns can be modeled by using a vertical autoregressive coefficient (β_2) of 1, i.e. complete correlation in the vertical direction. However, laboratory tests in samples from soil-cement mixed columns have shown that important heterogeneities are found in the sides as well as in the core of the columns [3]. The effect of different spatial correlations (e.g. magnitude of the correlation lengths and differences between the horizontal and the vertical correlations) could be interesting but it is out of the scope of this paper. Hence, it is worth highlighting that the quantitative recommendations of this study could vary for different correlation values.

The efficiency is measured in this analysis by the relative settlement of the structure with respect to free-field ($|u_z|$). The success function relating efficiency and effectiveness is presented in Fig. 7. It shows the box-and-whiskers plots for $|u_z|$ as a function of for two motions: EQ1 and EQ4. The mean values are linked by the dashed lines, the boxes correspond to the 3 quartiles of data and the whiskers are the lowest and highest data within 1.5 times the inter-quartile range. Additionally, the results for two different mesh discretizations are shown.

Firstly, it can be seen that for both motions the mean settlement is reduced as more treated soil is added, i.e. as decreases. However, the rate or slope is not constant and differs for the two motions. For EQ1 for instance, it seems that even a small amount of treated soil (e.g. $\gamma = 0.9$) can reduce, in average, the relative settlement. In contrast, it appears that about $\gamma = 0.2 - 0.4$, the average settlement will not be greatly affected if a greater amount of treated soil is used. However, for EQ4 the curvature is different and the plateau is mostly seen for lower values. Regarding the variation for each value, i.e. with respect to the different spatial distributions, it can be observed that higher variation is present for equal to 0.5 and 0.4, respectively. This value could be the percolation threshold dividing the two curves, from which the interactions between the two soils change. This aspect is further analyzed in Section 3.2.

Concerning, the effect of the mesh discretization, it was analyzed by reducing the element size in the horizontal direction by half for the entire FEM. As expected, the average $|u_z|$ is slightly higher with the fine mesh for almost all values tested. However, the difference in the mesh discretization appears to affect all the spatial fractions similarly. In comparison the variation for each value is only slightly reduced with the fine mesh and is mostly noted for EQ4. Given that the results were

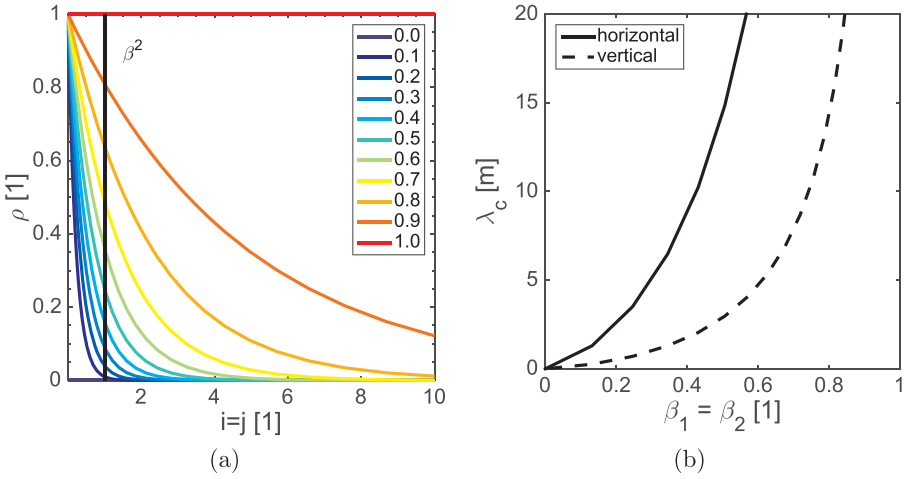

Fig. 6. Binary random field for $\beta_1 = \beta_2$: (a) autocorrelation function with i = j and (b) relation of β with the correlation length (λ_c) of an exponential function.

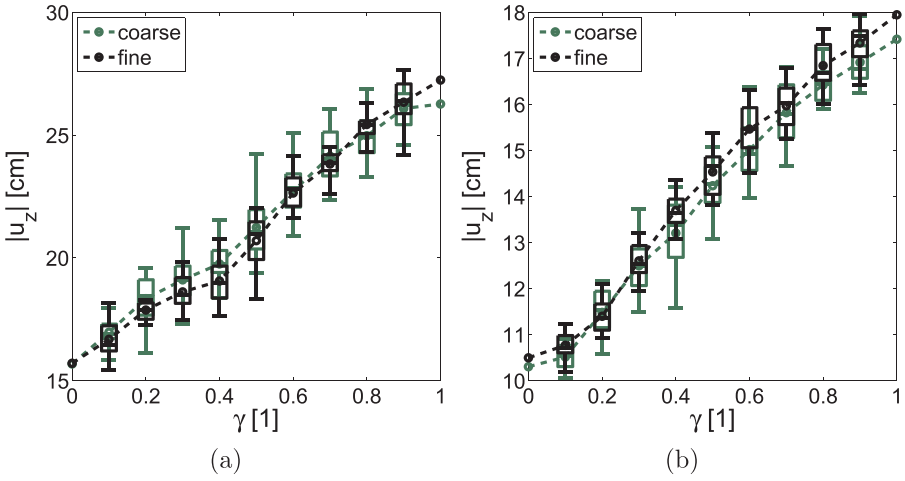

Fig. 7. Box-and-whiskers plot for the success function with (a) EQ1 and (b) EQ4. The effect of the mesh size is also shown.

not greatly changed, specially the shape of the success function, and that the numerical cost of the fine mesh is significantly higher, the coarse mesh will be used for the rest of the analyses.

3.1. Permeability and soil type effect

In order to understand the effect of the added spatial variability, some changes in the soils were tested. Principally, the effect of the permeability was analyzed. For the input motion, EQ1 was used. As was noted, the two soils have different soil parameters, among them, different hydraulic conductivity (κ). Montoya-Noguera and Lopez-Caballero [2], among others, showed that the pore pressure migration plays an important role in the effect of the spatial variability on $|u_z|$. The excess pore pressure (Δp_w) generation is related to the state of the soil with respect to the critical state, i.e. the dilatant or contractant tendency. Additionally, Δp_w dissipation and redistribution is related to κ. Hence, different scenarios were tested and are summarized in Table 3 as three types: (1) two soils with the same soil parameters except for κ, in other words, spatial variability is only affecting κ; (2) all soil parameters are different except for κ; and (3) the same as the previous case but with different sets of κ values. In general, all the soil parameters are related, though when the permeability decreases, the other soil parameters decrease too. However, when a cementitious process is used the permeability can be varied, while leaving the other soil parameters practically unchanged.

In Fig. 8a, the mean values and the one standard deviation envelope of the previously used soil mixture with different soil parameters (LMS and MDS) are compared to the first scenario where only LMS soil parameters are used and denotes the spatial fraction of κ equal to 10^{-4} m/s (corresponding to that of the LMS). The initial mixture, shown in purple, presents the highest reduction of about 40%. The first case corresponds to a 5% Bentonite permeation on sand, shown in orange, which as measured by Gueddouda et al. [53] produces a decrease in κ of one order of magnitude (i.e. for this case, $\kappa = 10^{-5}$ m/s). Results show that if the whole treated area is changed, the settlement is increased by less than 10%. Compared to the initial case, it can be seen that for the soils tested, the permeability has a much lower effect than the dilatant tendency. Additionally, a 10% Bentonite inclusion was modeled as a decrease of two orders of magnitude and is shown in brown. The average effect as well as the variation on the spatial variability was almost the same for both cases.

If however, κ is increased in one order of magnitude due to inclusions of a more coarser material, shown in red, the settlement decreases 20%. In this case, the effects are noticeable even for small fractions of inclusions ($\gamma = 0.8$), up to which the results are similar than those of the initial mixture. If both the dilatant tendency and the permeability increase, the settlement could be further decreased.

Table 3
Cases tested for permeability and soil type.

ID	Soil 1	Soil 2	κ_1 m/s	κ_2 m/s
	LMS	MDS	$1 \cdot 10^{-4}$	$1 \cdot 10^{-5}$
	LMS	LMS	$1 \cdot 10^{-4}$	$1 \cdot 10^{-5}$
	LMS	LMS	$1 \cdot 10^{-4}$	$1 \cdot 10^{-6}$
	LMS	LMS	$1 \cdot 10^{-4}$	$1 \cdot 10^{-3}$
	LMS	MDS	$1 \cdot 10^{-4}$	$1 \cdot 10^{-4}$
	LMS	MDS	$1 \cdot 10^{-4}$	$1 \cdot 10^{-3}$

Thus, in Fig. 8b, two additional scenarios are shown: the opposite case is shown in light blue, which is increasing the dilatant tendency while κ is kept constant; and in olive green, the soil parameters change and for this case κ_2 is higher. For the former, the results are similar to those of the original mixture until half the soil is changed (i.e. $\gamma = 0.5$). For lower spatial fractions, the decrease in settlement is lower. Once more, κ shows little effect on the settlement of spatial variable soil. However, when κ_2 equals to 10^{-3} m/s, Δp_w is easily dissipated and the soil improvement is slightly more efficient, as the settlement reduction is more than 45% for $= 0$. Concerning the different spatial fractions tested, it can be noted that significant changes in the average value are only seen for below 0.7 for a lower κ and below 0.5 for a higher one. In other words, it seems that for high values the response is mainly controlled by the original soil. However, as shown in Fig. 8a, if only κ is changed the system response is affected even when a small amount of treated soil is added (i.e. for about 0.8).

As the difference in κ is mainly observed in the pore pressure generation and dissipation, Fig. 9a shows the time evolution of the liquefaction ratio (i.e. $r_u(t) = \Delta p_w(t)/\sigma'_{v0}$ under the structure right column and at 3 m depth for the MDS case, that is where all the treated area has been replaced and $\gamma = 0$. The interaction between the soils is evidenced as r_u starts increasing after the predominant duration, i.e. $t > t_{95}$ [54], for almost all soils as consequence of the pore pressure migration from LMS at the surroundings. Concerning the highest κ (light red and lime), r_u does not increase at this depth because of the high rate of pore pressure dissipation. Hence the absolute relative settlement at the end of shaking is smaller than for other permeability values tested as shown in Fig. 9b. Once more, for κ equal to 10^{-5} m/s and 10^{-6} m/s, in orange and dark red, the response is very similar. In this figure, the input displacement time history is also shown in gray with a scaling factor of 50. It appears that the jumps on the settlement coincide in time with the

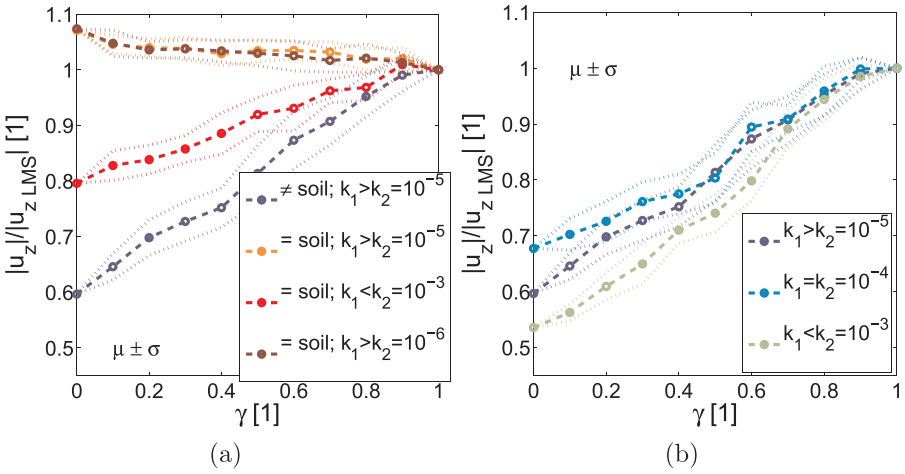

Fig. 8. Effect of the spatial variability of different soil parameters on $|u_z|$ with EQ1: a) when only the permeability varies and b) when various soil parameters vary. Mean (dashed lines) and the envelope of one standard deviation (dotted lines).

displacement peaks, shown as vertical dashed lines. Thus, even when the soil behavior is different, the time evolution depends greatly on the input displacement.

For all cases shown, it appears that the contractant or dilatant tendency of the soil's used has a greater effect than the change in permeability. Nonetheless, two important aspects are worth mentioning. In this analysis, focus was given to the co-seismic stage; whilst results for a post-seismic stage when all pore-pressure has been dissipated were also analyzed for some cases and the differences were less than 1%. Additionally, for the sake of brevity, results were only shown for the relative settlement of the structure with respect to free-field in order to take into account the soil-structure system and a typical engineering demand parameter. However, the effect of added spatial variability is different for other parameters, such as the liquefaction index on the soil deposit or surface Arias intensity as shown by Montoya-Noguera and Lopez-Caballero [2].

3.2. Homogenization theories

The success function of the soil improvement, defined by the mean $|u_z|$ values normalized by the value before treatment (i.e. the homogeneous LMS), for EQ1 is compared with the Wiener and HS bounds in Fig. 10a. This function is above all bounds tested which could be prejudicial for engineering design. As seen with the effect of other soil parameters, the relation of the settlement with appears to be related to either the response of one material or the other; in other words, it is mainly controlled by the interaction between the materials. The emergence of a percolation-like behavior is caused by the properties contrast and its effect in the response. For a highly heterogeneous system in the vicinity of the percolation threshold (γ_c), there are several local clusters that are mainly composed of the more stiffer material (MDS) which are the principal components of what becomes the percolating cluster.

Similarly, Fig. 10b shows the GEM equation fitted to the success function for EQ1. The percolation threshold and the scaling exponents were found by an optimization of the average $|u_z|$ of all values. The least-squares method was used and the variables were bounded between 0 and 1. The γ_c found is equal to 0.35, which is slightly below the values found in the literature for transport properties. This result is expected given the correlation in both directions and the important interactions between the soils shown previously. The scaling exponents s and t are equal to 0.24 and 0.21, respectively. As these are similar, the effect of having very high or very low is relatively similar. In other words, the system is affected for even a small amount of spatial

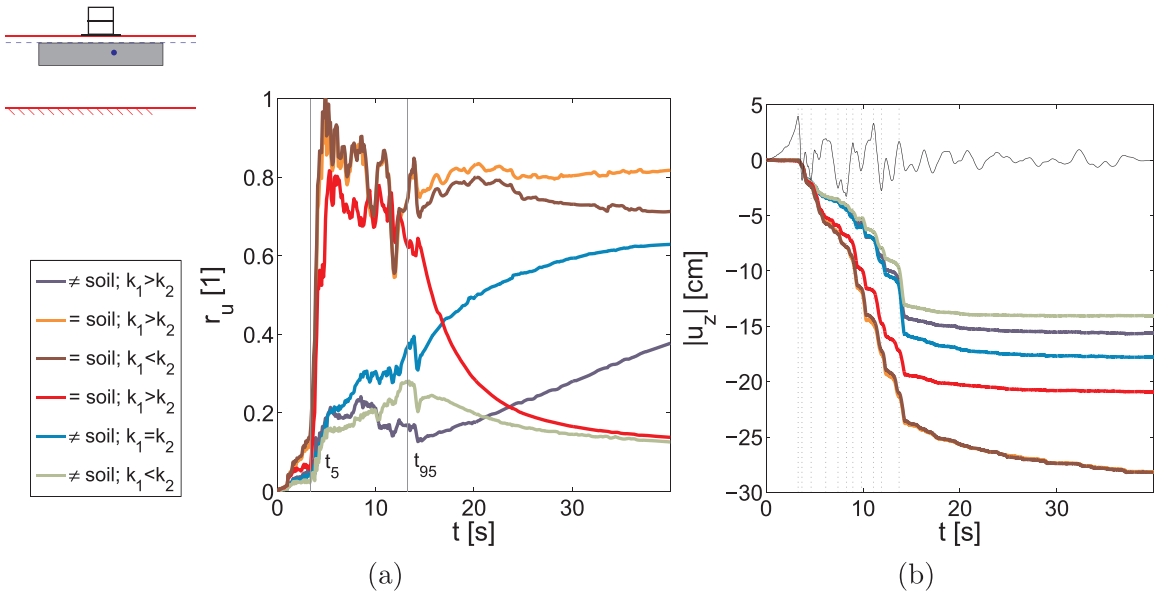

Fig. 9. Time evolution for different soil parameters of (a) liquefaction ratio and (b) $|u_z|$ with the input displacement time history of EQ1 shown with a scaling factor of 50. Vertical dashed lines show the displacement peaks. A description of soil parameters is shown in Table 3.

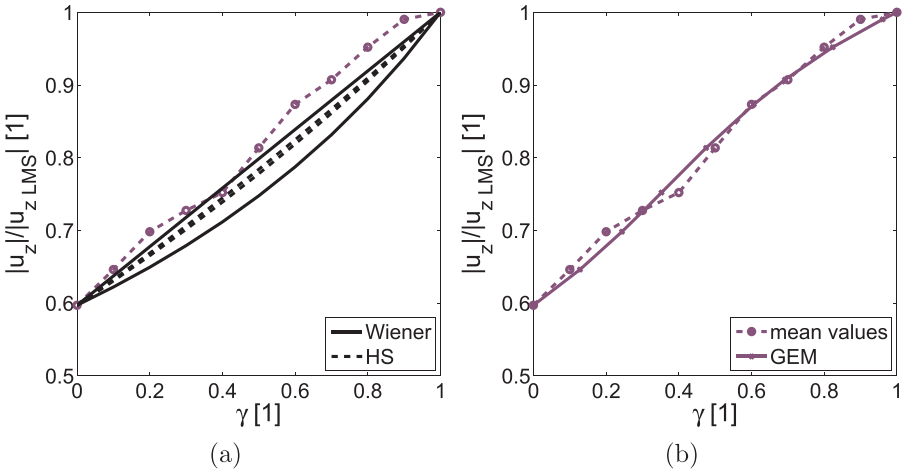

Fig. 10. Homogenization theories compared to the success function for the original LMS – MDS soil mixture with EQ1: (a) traditional theories and (b) generalized effective medium (GEM) equation.

variability. For this case the GEM equation gives a well suited fit for the success function, which is related to the theory of the percolation threshold, i.e. that after a certain value, there is a well-connected cluster that connects opposite sides of the system.

The success functions for the eight motions tested are shown in Fig. 11a. It is noted that the effect of the spatial variability varies greatly. As for each input motion, the $|u_z|$ is different for the extreme cases (i.e. $\gamma = 1$ and 0), the relative difference defined as $\Delta|u_z| = (|u_z| - |u_{z\,MDS}|)/(|u_{z\,LMS}| - |u_{z\,MDS}|)$ is shown in Fig. 11b. Note that the shape of the function, i.e. positive or negative concavity or s shape, appears to be related to other factors than only the initial $|u_z|$ value. For instance, EQ2 and EQ7 have a similar $|u_z|$ for the non-treated case however the former presents a positive concavity and the latter a negative one. This shape is related to the interactions between the two soils, though when the addition of a small fraction of treated soil affects only slightly the response and then for low values it drops, the relation has a positive concavity as for EQ2 and EQ5. In the other hand, when by only adding a small fraction, the settlement is drastically reduced while it is not greatly affected by low values, the relation has a negative concavity as for EQ3 and EQ7. Concerning the other motions, a combination of both interactions is identified.

Furthermore, Fig. 11c shows the normalized $|u_z|$ with respect to the case before treatment (i.e. LMS). The average values are shown in dashed lines. Additionally, the GEM equation was calibrated for all motions following the same procedure as for EQ1. The resulting curves are shown in Fig. 11c as solid lines and the values found are shown in Table 4.

The GEM equation gives a well suited fit for the effective settlement of the structure under the earthquake motions tested. Note that EQ1 and EQ4 have a similar normalized response and thus similar coefficients. Once more it appears that in this case the response is not only depending on the values of the extreme cases. For instance, even if EQ3 and EQ5 have similar $|u_z|$ ratio between the extreme cases (i.e. $|u_{z\,MDS}|/|u_{z\,LMS}|$) as shown in Fig. 11c, the effect for varying values is very different. Additionally, the percolation threshold does not seem to depend on $|u_{z\,MDS}|/|u_{z\,LMS}|$, as seen for EQ2 and EQ6.

In an effort to understand the relation between the input motion and the effect of the different spatial fractions, the value $\Delta|u_z|$ for $\gamma = 0.5$ was compared to 15 intensity measures (IM) such as maxima, energy or duration of acceleration, velocity or displacement. Fig. 12 shows the relation with the two IM that presented the best relation: the peak horizontal velocity (PHV) and the period of equivalent harmonic wave ($T_{V/A}$). As it can be seen, the results appear to be closely related to the input PHV values except for three motions (EQ1, EQ4 and EQ8). The black line corresponds to a logarithmic fit without the outliers motions and the coefficient of determination is calculated without the latter. Besides the fact that these motions present the highest PHA and highest $|u_{z\,LMS}|$, EQ1 and EQ8 were the only ones to be identified as pulse-like according to the procedure defined by Baker [55]. Additionally, EQ4 was recorded in medium-stiff soil, with a $V_{s\,30}$ below 400 m/s and presents low frequency content. This motion was not identified as pulse-like by Baker [55] procedure but it could be according to another

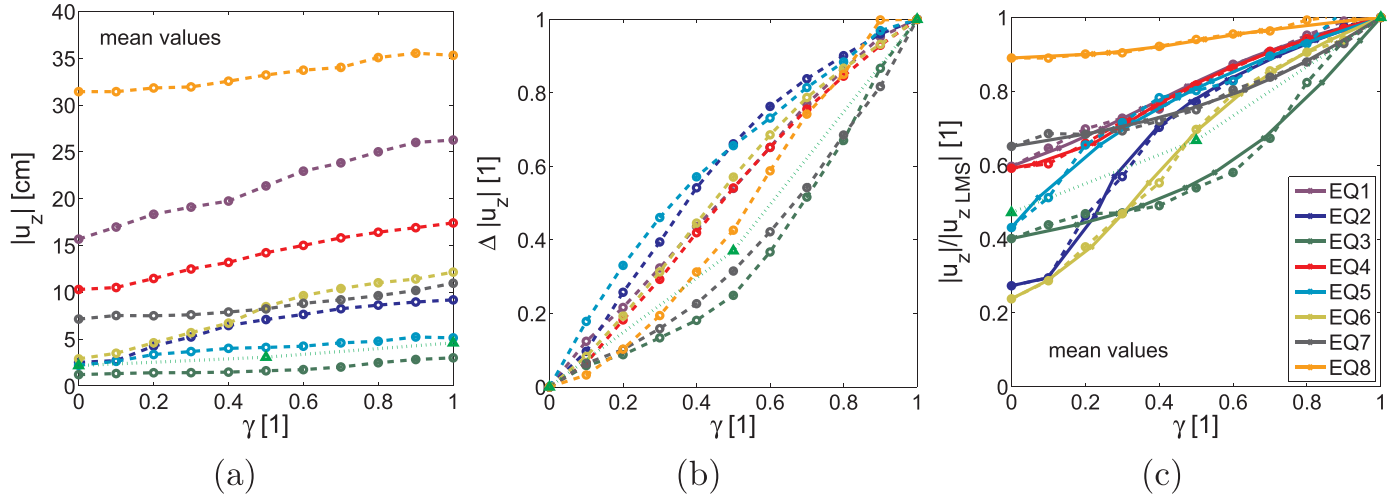

Fig. 11. $|u_z|$ relation with γ for earthquake motions (EQ) from 1 to 8: (a) mean values, (b) relative difference and (c) normalized mean values compared to GEM equation. Refer to Table 1 for EQ identification and some intensity measures.

Table 4
Calibration of GEM parameters.

	s	t	γ_c
EQ1	0.24	0.21	0.35
EQ2	0.1	0.26	0.18
EQ3	0.54	0.99	0.53
EQ4	0.14	0.19	0.3
EQ5	0.31	0.29	0.1
EQ6	0.73	0.3	0.44
EQ7	0.59	0.94	0.76
EQ8	0.02	0.08	0.1

definition of pulse-like developed by Dickinson and Gavin [56]. According to Kramer [57], the PHV is more likely to characterize ground-motion accurately at intermediate frequencies because it is less sensitive to the lower frequency components.

Fig. 12b shows $\Delta|u_z|$ for $\gamma = 0.5$ as a function of $T_{V/A}$, which gave the highest efficiency of all IM tested taking into account all motions. $T_{V/A}$ is the equivalent period corresponding to the intersection of the constant spectral acceleration and spectral velocity and is computed by:

$$T_{V/A} = 2\pi \frac{\alpha_V(\xi = 5\%)}{\alpha_A(\xi = 5\%)} \frac{PHV}{PHA} \quad \text{with} \quad \frac{\alpha_V(\xi = 5\%)}{\alpha_A(\xi = 5\%)} = \frac{1.65}{2.12} \tag{4}$$

where α_V and α_A are the Newmark-Hall median spectrum amplification factors for the constant velocity and the constant acceleration regions with 5% damping. Green and Cameron [58] found a close relation between this IM and the amplification of soft soil sites. In this case, $T_{V/A}$ appears to better describe $\Delta|u_z|$ for $\gamma = 0.5$ as it takes into account the PHV as well as the inverse of the PHA. According to Kawase [59], $T_{V/A}$ is a simplified indicator of the dominant period of the motion which appears to be related to the potential damage of structures. The PHV is commonly related to the shear strain demand of the motion and PHA, to its shear stress; hence their ratio can be related to the inverse of the stiffness modulus. The logarithmic fit was evaluated for all motions and even though the coefficient of determination is closer to unity for PHV, in the latter not all motions were taken into account. In Fig. 12b, the predominant period of the soil (T_0) and the structure (T_{str}^{FB}) is shown in solid and dashed lines, respectively. The differences of EQ3 and EQ5 with respect to the general trend can be due to the resonance with the soil for these motions.

Lastly, an additional motion was used to test only the relation of $\Delta|u_z|$ for $\gamma = 0.5$ with the different IM. It corresponds to the Loma Prieta earthquake of 1989 and identified as EQ9. This motion is also classified as non-pulse like according to Baker [55]. Fifty simulations were performed and the mean value is shown as a green triangle in Figs. 11 and 12. As it can be seen, this additional motion agrees well with the trend found by logarithmic fit for PHV and $T_{V/A}$.

4. Conclusions

In order to evaluate the success of a soil improvement technique considering the added spatial variability, a homogenization method is proposed in this study. A numerical model of discrete spatial heterogeneity was used to analyze the effect of added spatial variability caused by soil improvement. This effect was then quantified by assessing the liquefaction induced settlement of a fully nonlinear soil-structure system. Correlation in both directions was introduced by the nearest-neighbor model. The success of the soil improvement was evaluated as the relation between the spatial fraction of the treated-untreated soil mixture, known as the effectiveness, and the reduction of the liquefaction induced settlement, known as efficiency. An expanded set of soil material combinations and various input earthquake motions were tested. The following conclusions are obtained:

- The effect of added spatial variability was only slightly affected by the change in spatial discretization but depends greatly on the contractant or dilatant behavior of the soils used.
- For all motions tested, the fully-treated soil reduces the relative settlement of the structure with respect to free-field but the efficiency of the soil improvement, that is, the reduction on this relative settlement, varies for each input motion.
- It was shown that the success of the soil improvement is dependent on the input motion used and its resulting different interactions within the deposit.
- In the success function there is a level of treatment for which the settlement is drastically reduced, known as percolation threshold. For some motions, the addition of a small fraction of treated soil affects only slightly the response and for others this same fraction is highly efficient.
- Traditional homogenization models will in general overestimate the average efficiency related to the effectiveness of the soil improvement; however the generalized-effective-medium (GEM) equation including the percolation theory can describe this success function.
- This relation appears to depend on the period of equivalent harmonic wave ($T_{V/A}$) of the input motion which could be inversely related to the shear stiffness demand of the motion because it is directly proportional to PHV, commonly used as a shear strain

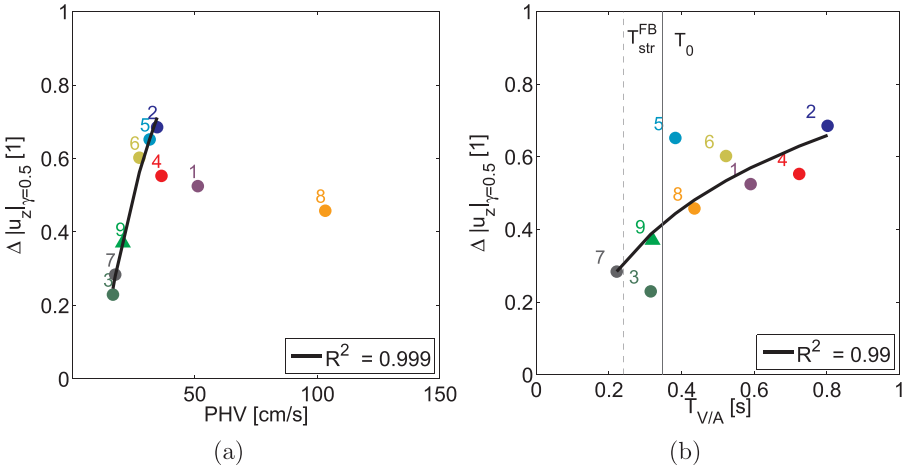

Fig. 12. Relation of the relative difference for $\gamma = 0.5$ and different IM: (a) I_A, (b) PHV and b) $T_{V/A}$. The earthquake motion's number is shown beside each value, refer to Table 1 for more information.

proxy, and inversely proportional to PHA, a shear stress proxy.

Soil improvement techniques have still to be further studied. This study highlights the importance of the spatial variability introduced to the soil. However, it could be enriched by the total coupling of FEM with the inherent spatial variability of the deposit and a model of the transport, permeation or injection process of the treated material in order to define the actual spatial distribution of the mixture. Doubtlessly, validation of the model with in-situ measurements or laboratory tests could contribute to this work but there is still a lack of measurements specially related to heterogeneous deposits.

Acknowledgment

The work described in this paper was partly supported by the SEISM Paris Saclay Research Institute. This support is gratefully acknowledged.

References

[1] Kasama K, Whittle A, Zen K. Effect of spatial variability on the bearing capacity of cement-treated ground. Soils Found 2012;52(4):600–19. http://dx.doi.org/10.1016/j.sandf.2012.07.003.
[2] Montoya-Noguera S, Lopez-Caballero F. Numerical modeling of discrete spatial heterogeneity in seismic risk analysis: application to treated ground soil foundation. GeoRisk: Assess Manag Risk Eng Syst Geohazards 2016;10(1). http://dx.doi.org/10.1080/17499518.2015.1058957 [Special issue: Modeling spatial variability in Geotechnical Engineering].
[3] Lambert S, Rocher-Lacoste F, Le Kouby A. Soil-cement columns, an alternative soil improvement method. in: Denies N., (ed.). ISSMGE - TC 211 International Symposium on Ground Improvement, vol. 3. Brussels, Belgium; 2012, p. 179- 188.
[4] Boulanger R, Idriss I, Stewart D, Hashash Y, Schmidt B. Drainage capacity of stone columns or gravel drains for mitigating liquefaction. In: Dakoulas P., Yegian M., Holtz R.D., editors. Geotechnical Earthquake Engineering and Soil Dynamics III; vol. 1. Seattle, Washington: ASCE; 1998, p. 678–690. Geotechnical Special Publication No. 75.
[5] DeJong JT, Mortensen BM, Martinez BC, Nelson DC. Bio-mediated soil improvement. Ecol Eng 2010;36(2):197–210. http://dx.doi.org/10.1016/j.ecoleng.2008.12.029.
[6] DeJong J, Soga K, Kavazanjian E, Burns S, van Paassen L, Fragaszy R, et al. Bio-and chemo-mechanical processes in geotechnical engineering. Geotechnique 2013;63(4):287–301.
[7] Burbank MB, Weaver TJ, Green TL, Williams BC, Crawford RL. Precipitation of calcite by indigenous microorganisms to strengthen liquefiable soils. Geomicrobiol J 2011;28(4):301–12. http://dx.doi.org/10.1080/01490451.2010.499929.
[8] Budiman JS, Mohammadi J, Bandi S. Effect of Large Inclusions on Liquefaction of Sand. Geotech Spec Publ 1995;56(1):48–63.
[9] Konrad JM, Dubeau S. Cyclic strength of stratified soil samples. In: Proceedings of the 55th Canadian Geotechnical Conference: Ground and Water: Theory to Practice. Niagara Falls, Canada; 2002, p. 89–94.
[10] Ghosh B, Madabhushi SPG. Effects of Localized Soil Inhomogeneity in Modifying Seismic Soil-Structure Interaction. In: Proceedings of the 16th ASCE Engineering Mechanics Conference. Seattle, WA; 2003.
[11] Chakrabortty P, Popescu R, Phillips R. Liquefaction of heterogeneous sand: centrifuge study. Geotech Test J 2010;33(4):1–11.
[12] Maharjan M, Takahashi A. Liquefaction Centrifuge Modeling in Non-homogeneous Soil Deposits. in: 15 WCEE. Lisboa, Portugal; 2012, p. 10.
[13] Koplik J. Homogenization and effective medium methods for transport in disordered granular systems. In: Bideau D, Dodds J, editors. Physics of granular media. New York, USA: NOVA Science Publishers; 1991. p. 215.
[14] Popescu R, Deodatis G, Nobahar A. Effects of random heterogeneity of soil properties on bearing capacity. Probabilistic Eng Mech 2005;20(4):324–41. http://dx.doi.org/10.1016/j.probengmech.2005.06.003.
[15] Wiener O. Die theorie des Mischkorpers fur das feld des stationaren Stromung. Erste Abhandlung die Mittelswertsatze fur Kraft, Polarisation un Energie. (german) [The theory of composites for the field of steady flow. First treatment of mean value estimates for force, polarization and energy]. Abh der Math-Phys Kl der Koniglich Sachs Ges der Wizzenschaften 1912;32(6):509–604.
[16] Hashin Z, Shtrikman S. A variational approach to the theory of the effective magnetic permeability of multiphase materials. J Appl Phys 1962;33(10):3125. http://dx.doi.org/10.1063/1.1728579.
[17] Frary M, Schuh Ca. Connectivity and percolation behaviour of grain boundary networks in three dimensions. Philos Mag 2005;85(11):1123–43. http://dx.doi.org/10.1080/14786430412331323564.
[18] Bunde A, Kantelhardt JW. Diffusion and conduction in percolation systems. In: Diffusion in Condensed Matter. Springer Science Business Media; 2005, p. 895–914. http://dx.doi.org/10.1007/3-540-30970-5_22.
[19] Brunini VE, Schuh CA, Carter WC. Percolation of diffusionally evolved two-phase systems. Phys Rev E 2011;83(2). http://dx.doi.org/10.1103/physreve.83.021119.
[20] Roman HE, Bunde A, Dieterich W. Conductivity of dispersed ionic conductors: a percolation model with two critical points. Phys Rev B 1986;34(5):3439–45. http://dx.doi.org/10.1103/physrevb.34.3439.
[21] McLachlan D, Blaskzkiewics M, Newnham R. Electrical resistivity of composites. J Am Ceram Soc 1990;73(8):2187–203.
[22] Sahimi M. Heterogeneous materials 1: linear transport and optical properties. New York: Springer; 2003. http://dx.doi.org/10.1007/b97507.
[23] Chen Y. Percolation and homogenization theories for heterogeneous materials. (Ph. D. Thesis); Massachusetts institute of technology; Massachusetts, USA; 2008.
[24] Mitchell J, Cooke H, Schaeffer J. Design considerations in ground improvement for seismic risk mitigation. In: Dakoulas P, Yegian M, Holtz RD. editors. Geotechnical Earthquake Engineering and Soil Dynamics III; vol. 1. Seattle, Washington: ASCE; 1998, p. 580–613. Geotechnical Special Publication No. 75.
[25] Zienkiewicz O, Taylor R. The Finite element method, solid and fluid mechanics, dynamics and non-linearity; vol. 2. London: McGraw-Hill Book Company; 4th ed.; 1991.
[26] Aubry D, Modaressi A. GEFDyn – manuel scientifique. France: LMSSMat: Ecole Centrale Paris; 1996.
[27] Foerster E, Modaressi H. A diagonal consistent mass matrix for earthquake site response simulations. In: Proceedings of the 4th International Conference on Earthquake Geotechnical Engineering (ICEGE). Thessaloniki, Greece; 2007a, p. 1–11. Paper: 1242.
[28] Marburg S. Computational Acoustics of Noise Propagation in Fluids - Finite and Boundary Element Methods; chap. Discretization Requirements: How many Elements per Wavelength are Necessary? Berlin, Heidelberg: Springer Berlin Heidelberg. ISBN 978-3-540-77448-8; 2008, p. 309–332. ⟨http://dx.doi.org/10.1007/978-3-540-77448-8_12⟩.
[29] Montoya-Noguera S, Lopez-Caballero F. Effect of coupling excess pore pressure and deformation on nonlinear seismic soil response. Acta Geotech 2016;11(1):191–207. http://dx.doi.org/10.1007/s11440-014-0355-7.
[30] Saez E, Lopez-Caballero F, Modaressi-Farahmand-Razavi A. Inelastic dynamic soil-structure interaction effects on moment-resisting frame buildings. Eng Struct 2013;51(1):166–77. http://dx.doi.org/10.1016/j.engstruct.2013.01.020.
[31] Modaressi H, Benzenati I. Paraxial approximation for poroelastic media. Soil Dyn Earthq Eng 1994;13(2):117–29.
[32] Zienkiewicz OC, Bicanic N, Shen FQ. Advances in Computational Nonlinear Mechanics; chap. Earthquake Input Definition and the Trasmitting Boundary Conditions. Vienna: Springer Vienna. ISBN 978-3-7091–2828-2; 1989, p. 109–138. ⟨http://dx.doi.org/10.1007/978-3-7091-2828-2_3⟩.
[33] Lopez-Caballero F, Modaressi-Farahmand-Razavi A. Numerical simulation of liquefaction effects on seismic SSI. Soil Dyn Earthq Eng 2008;28(2):85–98. http://dx.doi.org/10.1016/j.soildyn.2007.05.006.
[34] Sáez E, Ledezma C. Liquefaction mitigation using secant piles wall under a large water tank. Soil Dyn Earthq Eng 2015;79(B):415–28. http://dx.doi.org/10.1016/j.soildyn.2015.06.012.
[35] Ayoubi P, Pak A. Liquefaction-Induced Settlement of Shallow Foundations on Heterogeneous Subsoil. Soil Dyn Earthq Eng 2017;94(March):35–46. http://dx.doi.org/10.1016/j.soildyn.2017.01.004.
[36] Vechio F, Emara M. Shear deformation in reinforced concrete frames. Acids Struct J 1992;89(1):46–56.
[37] Aubry D, Modaressi H. Seismic wave propagation in soils including non-linear and pore pressure effects. In: Recent Advances in Earthquake Engineering and Structural Dynamics. France: Ouest Editions; 1985, p. 209-224. Edited by V. Davidovici.
[38] Modaressi H. Modélisation numérique de la propagation des ondes dans les milieux poreux anélastiques. (Ph.D. Thesis); Laboratoire MSSMat, Ecole Centrale Paris; Châtenay-Malabry, France; 1987. Advisor: Denis Aubry.
[39] Aubry D, Modaressi H. Un modele de sols satures en dynamique non lineaire. Rev Fr De Geotech 1989;46:43–75.
[40] Hujeux J. Une loi de comportement pour le chargement cyclique des sols. in: Génie Parasismique. France: Presses ENPC; 1985, p. 278-302. Edited by V. Davidovici.
[41] Costa D'Aguiar S, Modaressi-Farahmand-Razavi A, Dos Santos J, Lopez-Caballero F. Elastoplastic constitutive modelling of soil structure interfaces under monotonic and cyclic loading. Comput Geotech 2011;38(4):430–47. http://dx.doi.org/10.1016/j.compgeo.2011.02.006.
[42] Foerster E, Modaressi H. Nonlinear numerical methods for earthquake site response analysis II- case studies. Bull Earthq Eng 2007;5(3):325–45. http://dx.doi.org/10.1007/s10518-007-9034-5.
[43] Bernardie S, Foerster E, Modaressi H. Non-linear site response simulations in Chang-Hwa region during the 1999 Chi-Chi earthquake, Taiwan. Soil Dyn Earthq Eng 2006;26:1038–48. http://dx.doi.org/10.1016/j.soildyn.2006.02.004.
[44] Sica S, Pagano L, Modaressi A. Influence of past loading history on the seismic response of earth dams. Comput Geotech 2008;35(1):61–85. http://dx.doi.org/10.1016/j.compgeo.2007.03.004.
[45] Lopez-Caballero F, Modaressi-Farahmand-Razavi A, Modaressi H. Nonlinear numerical method for earthquake site response analysis i - elastoplastic cyclic model and parameter identification strategy. Bull Earthq Eng 2007;5(3):303–23. http://dx.doi.org/10.1007/s10518-007-9032-7.
[46] Carrilho Gomes R, Santos J, Modaressi-Farahmand Razavi A, Lopez-Caballero F. Validation of a strategy to predict secant shear modulus and damping of soils with an elastoplastic model. KSCE J Civil Eng 2016;20(2):609–22. http://dx.doi.org/10.1007/s12205-015-0516-8.
[47] Lopez-Caballero F, Modaressi-Farahmand-Razavi A. Numerical simulation of mitigation of liquefaction seismic risk by preloading and its effects on the performance of structures. Soil Dyn Earthq Eng 2013;49(1):27–38. http://dx.doi.org/10.1016/j.soildyn.2013.02.008.
[48] Saez E. Dynamic non-linear soil structure interaction. (Ph.D. Thesis); Ecole Centrale Paris; France; 2009.

[49] El Mohtar CS, Bobet A, Santagata MC, Drnevich VP, Johnston CT. Liquefaction mitigation using bentonite suspensions. J Geotech Geoenviron Eng 2013;139(8):1369–80. http://dx.doi.org/10.1061/(asce)gt.1943-5606.0000865.
[50] Bartlett M, Besag J. Correlation Properties of Some Nearest-Neighbor Models. Bull Int Stat Inst 1969;43(2):191–3.
[51] Alonso E, Krizek R. Stochastic formulation of soil properties. In: Proceedings of the 2nd International Conference on Applications of Statistics and Probability in Soil and Structural Engineering; vol. 2. Aachen; 1975, p. 9–32.
[52] Senger R, Lucia F, Kerans C, Ferris M, Fogg CE. Geostatistical/ GeologicalPermeability Characterization of Carbonate Ramp Deposits in Sand Andres Outcrop, Algerita Escarpment, New Mexico. In: Permian Basin Oil and Gas Recovery Conference. Midland, Texas; 1992, p. 287-301.
[53] Gueddouda M, Lamara M, Abou-bekr N, Taibi S. Hydraulic behaviour of dune sand bentonite mixtures under confining stress. Geomech Eng 2010;2(3):213–27. http://dx.doi.org/10.12989/gae.2010.2.3.213.
[54] Trifunac M, Brady A. A study on the duration of strong earthquake ground motion. Bull Seismol Soc Am 1975;65(3):581–626.
[55] Baker JW. Quantitative classification of near-fault ground motions using wavelet analysis. Bull Seismol Soc Am 2007;97(5):1486–501. http://dx.doi.org/10.1785/0120060255.
[56] Dickinson BW, Gavin HP. Parametric statistical generalization of uniform-hazard earthquake ground motions. J Struct Eng 2011;137(3):410–22. http://dx.doi.org/10.1061/(asce)st.1943-541x.0000330.
[57] Kramer S. Geotechnical earthquake engineering. 1st ed. New Jersey, United States of America: Prentice-Hall; 1996.
[58] Green R, Cameron W. The influence of ground motion characteristics on site response coefficients. In: Pacific conference on earthquake engineering. University of Canterbury, Christchurch, New Zealand: New Zealand Society for Earthquake Engineering; 2003, p. 19. Paper No. 90 on CD.
[59] Kawase H. Strong ground motion characteristics and their damage impact to structures during the off pacific coast of tohoku earthquake of march 11, 2011; How extraordinary was this M9.0 earthquake? In: Proceedings of the 4th IASPEI / IAEE International Symposium: Effects of Surface Geology on Seismic Motion. University of California Santa Barbara; 2011, p. 13.